ANALYSIS OF DIELECTRIC WAVEGUIDE BENDS AND CURVED COUPLER STRUCTURES USING FINITE DIFFERENCE BEAM PROPAGATION METHOD

A THESIS

SUBMITTED TO THE DEPARTMENT OF ELECTRICAL AND ELECTRONICS ENGINEERING

AND THE INSTITUTE OF ENGINEERING AND SCIENCES

OF BILKENT UNIVERSITY

IN PARTIAL FULFILLMENT OF THE REQUIREMENTS

FOR THE DEGREE OF

MASTER OF SCIENCE

By

Erdem Ofli

July 1997

ANALYSIS OF DIELECTRIC WAVEGUIDE BENDS AND CURVED COUPLER STRUCTURES USING FINITE DIFFERENCE BEAM PROPAGATION METHOD

A THESIS

SUBMITTED TO THE DEPARTMENT OF ELECTRICAL AND

ELECTRONICS ENGINEERING

AND THE INSTITUTE OF ENGINEERING AND SCIENCES

OF BILKENT UNIVERSITY

IN PARTIAL FULFILLMENT OF THE REQUIREMENTS

FOR THE DEGREE OF

MASTER OF SCIENCE

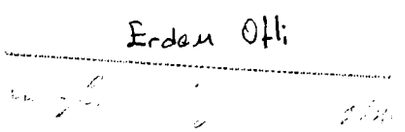

By

Erdem Ofli

July 1997

I certify that I have read this thesis and that in my opinion it is fully adequate, in scope and in quality, as a thesis for the degree of Master of Science.

Prof. Dr. Ayhan Altıntaş(Supervisor)

I certify that I have read this thesis and that in my opinion it is fully adequate, in scope and in quality, as a thesis for the degree of Master of Science.

Assoc. Prof. İrşadi Aksun

I certify that I have read this thesis and that in my opinion it is fully adequate, in scope and in quality, as a thesis for the degree of Master of Science.

Assoc. Prof. Gönül Turhan Sayan

I certify that I have read this thesis and that in my opinion it is fully adequate, in scope and in quality, as a thesis for the degree of Master of Science.

Dr. Vladimir Yurchenko

Approved for the Institute of Engineering and Sciences:

Prof. Dr. Mehmet Baray
Director of Institute of Engineering and Sciences

ABSTRACT

ANALYSIS OF DIELECTRIC WAVEGUIDE BENDS AND CURVED COUPLER STRUCTURES USING FINITE DIFFERENCE BEAM PROPAGATION METHOD

Erdem Ofli
M.S. in Electrical and Electronics Engineering
Supervisor: Prof. Dr. Ayhan Altıntaş
July 1997

In this thesis, implicit finite difference beam propagation method based on Crank-Nicholson discretization procedure is implemented and applied to the analysis of propagation of optical beams in an orthogonal bend and a curved coupler structure. The efficiency factor which accounts for the power loss as a result of the bend is calculated for different waveguide width values and compared with analytic solutions in the analysis of the orthogonal bend. Also, the effect of the rotation of the etched semiconductor-air interface from its ideal position is examined. In the curved coupler analysis, the bend loss and the variation of power transfer ratios for different values of minimum distance that separates the branches of the structure are investigated and compared with analytic solutions. On both structure, the evolution of the Gaussian beam in the positive z-direction is obtained.

Keywords : Beam Propagation Method, Photonic Integrated Circuits, Waveguide Couplers, Optical Waveguide Bends.

ÖZET

SONLU FARKLAR DEMET YAYILIM YÖNTEMİ KULLANARAK YALITKAN DALGA KILAVUZU BÜKÜMLERİN VE BÜKÜLMÜŞ BAĞLAŞTIRICI YAPILARIN ÇÖZÜMLEMESİ

Erdem Ofli
Elektrik ve Elektronik Mühendisliği Bölümü Yüksek Lisans
Tez Yöneticisi: Prof. Dr. Ayhan Altıntaş
Temmuz 1997

Bu tezde, Crank-Nicholson parçalara bölme işlemine dayanan örtük sonlu farklar demet yayılım yöntemi gerçekleştirildi ve bir dikey büküm ve bir bükülmüş bağlaştırıcı yapıda optik demetlerin yayılımlarının çözümlemesine uygulandı. Dik büküm çözümlemesinde, farklı dalga kılavuzu genişlikleri için bükümden kaynaklanan güç yitimini sayan verim çarpanı hesaplandı ve analitik çözümlerle karşılaştırıldı. Ayrıca, dağlanmış yalıtkan-hava arayüzeyinin ülkül konumundan dönmesinin etkisi incelendi. Bükülmüş bağlaştırıcı çözümlemesinde, yapının dallarını ayıran en az uzaklığın farklı değerleri için büküm yitimi ve güç aktarım oranlarının değişimi araştırıldı ve analitik çözümlerle karşılaştırıldı. Her iki yapıda, artı z yönünde Gauss demetinin evrimi elde edildi.

Anahtar Kelimeler : Demet Yayılım Yöntemi, Fotonik Tümleşik Devreler, Dalga Kılavuzu Bağlaştırıcılar, Optik Dalga Kılavuzu Bükümler.

ACKNOWLEDGEMENT

I would like to express my deep gratitude to my supervisor Prof. Dr. Ayhan Altıntaş for his guidance, suggestions and valuable encouragement throughout the development of this thesis.

I would like to thank Assoc. Prof. İrşadi Aksun, Assoc. Prof. Gönül Turan Sayan and Dr. Vladimir Yurchenko for reading and commenting on the thesis and for the honor they gave me by presiding the jury.

I thank my friends Alper, Ayşin, Cem, Ebru, Evrim, Eylem, Gürhan and Murat, for everything.

Sincere thanks are also extended to my officemates Fatma, Fehmi and Moez.

To my family
and
my friends.

Contents

List of Figures

Chapter 1

Introduction

Integrated optics play an important role in the optical telecommunication and instrumentation applications. Such circuits use guided optical waves to perform various different functions such as switching, multiplexing, modulation and demodulation. Since the basic building block of photonic integrated circuits (PIC) is the optical waveguide, it is of great importance to have powerful and flexible tools to analyze, design and optimize dielectric waveguide structures. Such analysis and design methods will generate the computer aided design tools for PIC. So far, various different methods have been developed and applied to the analysis of waveguides. All these methods can be combined under two groups which are identified according to their appropriateness for z-invariant and z-variant structures.

In z-invariant waveguides, the cross-sectional dimensions and profiles do not vary along the direction of propagation (which is the z-direction) and they are analyzed by a simple method which is called the effective index method [1]. This

method is only valid for weakly guiding waveguides. Although it can still be used to design and analyze single-mode, strongly guiding waveguides, its accuracy degrades rapidly as the confinement of the mode increases. So, there is need for efficient numerical methods for strongly guiding structures . For such cases, the finite difference method and variational methods based on the Rayleigh-Ritz procedure are commonly used [2]. Finite elements methods have also been employed in the analysis of the optical waveguides [3].

Z-variant waveguides such as directional coupler, Y-junction and X-crossing waveguides, have cross-sectional dimensions and index profiles that vary along the propagation direction. The most commonly used method to analyze such structures is so-called Beam Propagation Method (BPM), which can also be applied to the analysis of z-invariant structures [4]. Conventional BPM requires the use of the fast Fourier Transform (FFT) at every propagation step. In FFT Beam Propagation Method (FFT-BPM), the effective index method is usually used to convert a three-dimensional geometry into an equivalent two-dimensional geometry. But if the refractive index in the waveguide cross-sectional profile varies rapidly, one should use very small propagation steps [5],[6] resulting in a large computational time. To improve the computational efficiency of FFT-BPM, the finite difference techniques are used to approximate the plane wave propagation operator [7],[8],[9]. In all these algorithms including FFT-BPM, the exact formal propagation operator is split into several operators. These operators describe the wave propagation in the medium and can be realized using the FFT algorithm, or the split-step implicit finite difference procedure or the real-space algorithm. In the FFT algorithm, each plane wave component of the field is calculated using FFT. Then, each plane wave component is propagated and at the end of the

propagation step, the resulting field in the real space is found using inverse FFT [4],[9]. In the split-step finite difference procedure, the field propagation in the x-direction is considered while the y coordinate is kept constant. Then, the field propagation in y-direction is calculated keeping the x coordinate constant. In this method, it is possible to use the Crank-Nicholson algorithm resulting tridiagonal linear equations that can be solved very efficiently [7],[9]. In the real-space algorithm, the propagation in x-direction is calculated by multiplying a field column vector at each constant y position with a series of unitary block diagonal matrices. Then, the propagation in y-direction is obtained similarly [8],[9].

In another approach, the finite difference techniques are directly applied to the paraxial wave equation, which results in the finite difference beam propagation method (FD-BPM) [10],[11]. In this method, operator algorithm, hence operator splitting is not used. As in the case of FFT-BPM, a three-dimensional structure can be converted to a two-dimensional structure by using the effective index method. For two-dimensional geometries, inherently stable and unitary Crank-Nicholson finite difference techniques can be used resulting in a very efficient, stable and power-conserving algorithm [10]. However, for three-dimensional cases, this technique requires to convert a large matrix at every propagation step, rendering the algorithm to be inefficient and hence unattractive. To circumvent this difficulty, an explicit finite difference BPM (EFD-BPM) was introduced and applied to the analysis of semiconductor rib Y-junctions [11]. Also, EFD-BPM incorporating a nonuniform mesh was formulated and applied to analyze several z-invariant and z-variant rib waveguides [12].

It is apparent that the scalar BPM totally ignores the vectorial nature of the

electromagnetic field, as a consequence, the polarization effects of the waveguide structures under study can not be modeled. For such cases, semi-vectorial BPM and fully Vectorial BPM schemes were developed [13],[14].

In this thesis, the FD-BPM algorithm is formulated and applied to two z-variant structures; an orthogonal bend and a curved coupler structure which are widely used as interconnects [15] or as passive components in integrated circuits. Investigation of bent losses and variation of power transfer ratios from the input waveguide to the output waveguide are important parameters in the design of curved coupler structures. FD-BPM has been successfully applied to the analysis of propagation in a bent dielectric waveguide [16]. However, to the best of author's knowledge no attempt has been made to analyze a curved coupler structure using this technique.

In Chapter 2, the implicit and explicit FD-BPM algorithm is outlined in detail. In addition effective index method is also explained in this chapter. An orthogonal bend structure is analyzed using both the Fields of Shadows Method and FD-BPM, and the results are compared in Chapter 3. In Chapter 4, the analysis of the curved coupler structure using FD-BPM is presented, and the results are compared with an approximate solution developed by Mittra [17]. The limitations and advantages of the method and further possible improvements are discussed in Chapter 5.

Chapter 2

Numerical Method

Numerical techniques are employed to rigorously solve differential, integro-differential and integral equations that cannot be solved by analytic techniques. With the advent of fast computers, these techniques have been computationally efficient and accurate as compared to approximate analytic techniques. In this chapter, the beam propagation method (BPM) which is one of the most suitable approaches to analyze arbitrary waveguide propagation problems is introduced. In particular, the finite-difference BPM (FD-BPM) is considered.

2.1 Beam Propagation Method (BPM)

A general way of handling electromagnetic wave propagation in integrated optics is to solve Maxwell's equations with appropriate boundary conditions. But

in such PIC, the ratio between the propagation distance and the transverse dimensions of the propagating energy is large. It is very difficult to implement the solution of Maxwell's equations with boundary conditions since it will use great computer memory and CPU performance. Fortunately, in most cases, the scalar wave equation is sufficient to describe the wave propagation in PIC. For waveguides with a step-index profile, i.e., $n = n_{co}$ in the core and $n = n_{cl}$ in the cladding, all items involving $\nabla_t(ln(n^2))$ in the vector wave equation vanish within the core and cladding. Consequently, within the core and cladding the scalar wave equation can be used approximately [18]. Also, they are paraxial, i.e., the phase fronts of guided waves are almost planar or their plane wave spectra are quite narrow. Finally, in many situations, index variations along the propagation direction (usually the positive z-direction) tend to be small and gradual. So, the wave amplitudes change slowly (slowly varying amplitude approximation) and back reflections are negligible. Under these conditions, the scalar wave equation,

$$\nabla^2\psi + k^2n^2(r)\psi = 0 \tag{2.1}$$

can be reduced to the paraxial wave equation,

$$2jk_on_o\frac{\partial\psi}{\partial z} = \frac{\partial^2\psi}{\partial x^2} + \frac{\partial^2\psi}{\partial y^2} + k_o^2[n^2(x,y,z) - n_o^2]\psi, \tag{2.2}$$

where n_o is a reference refractive index that describes the average phase velocity of the wave, k_o is the wave number in the vacuum and $\psi(x,y,z) = \phi(z)U(x,y)$. The reference refractive index determines the rapidly varying component of the wave and ψ represents the slowly varying amplitude along the propagation direction. So, electric field can be written as follows,

$$E(x,y,z) = \psi(x,y,z)exp(-jk_on_oz). \tag{2.3}$$

To get accurate results, the reference refractive index value must be carefully chosen. In guided-wave problems, it is usually chosen as the index of the substrate if the difference between refractive indices of the film and the substrate is small.

Using paraxial wave equation, an initial value problem is described. One can start with an arbitrary initial wave amplitude, $\psi(x, y, 0)$, which could be a Gaussian beam formed by a lens, and find the resulting amplitude Δz away by integrating the paraxial wave equation over Δz. This procedure is repeated to find the evolution of the initial field over the PIC. The field values at $z = 0$ are enough to calculate the field values at $z = \Delta z$. In other words, there is no need to store or manipulate the field values at every grid point in the z-direction as required in the solution of boundary value problem. Thus, BPM is computationally much more efficient. Also, all parts of the wave which includes the guided and radiation spectrum, are handled at the same time, i.e., there is no need for modal decomposition or to neglect the radiation part of the spectrum. But, since it uses the paraxial wave equation, back reflections and the wide-angle propagation are not handled.

Conventional BPM requires fast Fourier transform (FFT) at every propagation step [5]. FFT-BPM which involves operator techniques, is usually combined with the effective index method to convert three dimensional structure to an equivalent two dimensional geometry. Recently, it has been shown that much more efficient and robust algorithms can be generated by using finite difference techniques [9]. Due to its significant advantages, only the finite difference BPM (FD-BPM) will be described here. It is possible to generate FD-BPM algorithms using implicit or explicit techniques. Here, both approaches based on the Crank-Nicholson algorithm [19] will be briefly described.

2.2 Implicit Finite Difference Beam Propagation Method (FD-BPM)

The idea behind the implicit FD-BPM is to approximate the paraxial wave equation (2.2) using finite difference techniques. It requires a computational window in the transverse dimensions (x, y) and a grid in the z-direction. With the computational window and z-grid appropriately chosen, we then have $x = p\Delta x$, $y = q\Delta y$, $z = l\Delta z$ where p, q and l are integers defining the grid location. Crank-Nicholson algorithm is chosen to approximate x and y derivatives in the paraxial wave equation since it is both unconditionally stable and unitary . The details of the algorithm are given in Appendix A. A straightforward implementation of the FD-BPM can lead to an unstable algorithm which allows slight round-off errors to lead to nonphysical results. With Crank-Nicholson scheme, fields will not diverge without any physical reason regardless of the mesh size, Δx, Δy, Δz. But, accuracy will be lost as the mesh size gets larger.

Assuming $\psi(x, y, z) = \psi^l_{p,q}$ and approximating the z-partial on the left side of the paraxial wave equation, we obtain

$$\frac{\partial \psi}{\partial z} = \left[\frac{\psi^{l+1}_{p,q} - \psi^l_{p,q}}{\Delta z}\right]. \tag{2.4}$$

The derivatives with respect to x and y on the right-hand side are approximated using finite-difference approximations. By taking the average of the discretization at $z = l\Delta z$ and $z = (l+1)\Delta z$, we obtain

$$\frac{\partial^2 \psi}{\partial x^2} = \frac{1}{2}\left[\frac{\psi^{l+1}_{p+1,q} - 2\psi^{l+1}_{p,q} + \psi^{l+1}_{p-1,q}}{\Delta x^2} + \frac{\psi^{l}_{p+1,q} - 2\psi^{l}_{p,q} + \psi^{l}_{p-1,q}}{\Delta x^2}\right], \tag{2.5}$$

$$\frac{\partial^2\psi}{\partial y^2} = \frac{1}{2}\left[\frac{\psi^{l+1}_{p,q+1} - 2\psi^{l+1}_{p,q} + \psi^{l+1}_{p,q-1}}{\Delta y^2} + \frac{\psi^{l}_{p,q+1} - 2\psi^{l}_{p,q} + \psi^{l}_{p,q-1}}{\Delta y^2}\right]. \tag{2.6}$$

For the final term in the paraxial wave equation, one can write

$$k_o^2(n^2 - n_o^2)\psi = k_o^2\left[\frac{(n^{l+1}_{p,q})^2 + (n^{l}_{p,q})^2}{2} - n_o^2\right]\left(\frac{\psi^{l+1}_{p,q} + \psi^{l}_{p,q}}{2}\right). \tag{2.7}$$

To normalize, we divide the whole equation by k_0^2 and use $k_0\Delta z = \Delta Z$, $k_0\Delta x = \Delta X$ and $k_0\Delta y = \Delta Y$. Then, substituting (2.4) through (2.7), we obtain

$$\begin{aligned} -\frac{\psi^{l+1}_{p-1,q}}{2\Delta X^2} + [-b\psi^{l+1}_{p,q-1} + a_{p,q}\psi^{l+1}_{p,q} - b\psi^{l+1}_{p,q+1}] - \frac{\psi^{l+1}_{p+1,q}}{2\Delta X^2} \\ = \frac{\psi^{l}_{p-1,q}}{2\Delta X^2} + [b\psi^{l}_{p,q-1} + c_{p,q}\psi^{l}_{p,q} + b\psi^{l}_{p,q+1}] + \frac{\psi^{l}_{p+1,q}}{2\Delta X^2}, \end{aligned} \tag{2.8}$$

where

$$\begin{aligned} b &= \frac{1}{2\Delta Y^2}, \\ a_{p,q} &= \frac{2jn_o}{\Delta Z} + \frac{1}{\Delta X^2} + \frac{1}{\Delta Y^2} - \frac{1}{2}\left[\frac{(n^{l+1}_{p,q})^2 + (n^{l}_{p,q})^2}{2} - n_o^2\right], \\ c_{p,q} &= -a_{p,q} + \frac{4jn_o}{\Delta Z}. \end{aligned}$$

PxQ equations are obtained at each z step for $p = 1$ to P and $q = 1$ to Q within the computational window. The solution of these equations is best handled with matrices.

We define a vector which encompasses y for each x position, p:

$$\Psi^l_p = \begin{bmatrix} \psi^l_{p,1} \\ \vdots \\ \psi^l_{p,Q} \end{bmatrix}. \tag{2.9}$$

Then, we can group common p indices into a matrix-difference equation along x:

$$-\mathbf{B}\Psi^{l+1}_{p-1} + \mathbf{A_p}\Psi^{l+1}_{p} - \mathbf{B}\Psi^{l+1}_{p+1} = \mathbf{B}\Psi^{l}_{p-1} + \mathbf{C_p}\Psi^{l}_{p} + \mathbf{B}\Psi^{l}_{p+1}, \tag{2.10}$$

where

$$\mathbf{B} = \frac{1}{2\Delta X^2}\mathbf{I},$$

$$\mathbf{A_p} = \begin{bmatrix} a_{p,1} & -b & 0 & & 0 & 0 \\ -b & a_{p,2} & -b & 0 & & 0 \\ 0 & -b & a_{p,3} & -b & 0 & \\ & 0 & & & & 0 \\ 0 & & 0 & -b & a_{p,Q-1} & -b \\ 0 & 0 & & 0 & -b & a_{p,Q} \end{bmatrix},$$

$$\mathbf{C_p} = \begin{bmatrix} c_{p,1} & b & 0 & & 0 & 0 \\ b & c_{p,2} & b & 0 & & 0 \\ 0 & b & c_{p,3} & b & 0 & \\ & 0 & & & & 0 \\ 0 & & 0 & b & c_{p,Q-1} & b \\ 0 & 0 & & 0 & b & c_{p,Q} \end{bmatrix}.$$

and $\mathbf{I}$ is the QxQ identity matrix. Writing all P equations (2.10) along x in matrix form, we obtain

$$\begin{bmatrix} \mathbf{A_1} & \mathbf{-B} & 0 & & 0 & 0 \\ \mathbf{-B} & \mathbf{A_2} & \mathbf{-B} & 0 & & 0 \\ 0 & \mathbf{-B} & \mathbf{A_3} & \mathbf{-B} & 0 & \\ & 0 & & & & 0 \\ 0 & & 0 & \mathbf{-B} & \mathbf{A_{P-1}} & \mathbf{-B} \\ 0 & 0 & & 0 & \mathbf{-B} & \mathbf{A_P} \end{bmatrix} \begin{bmatrix} \Psi_1^{l+1} \\ \Psi_2^{l+1} \\ \Psi_3^{l+1} \\ \vdots \\ \Psi_{P-1}^{l+1} \\ \Psi_P^{l+1} \end{bmatrix}$$

$$= \begin{bmatrix} \mathbf{C_1} & \mathbf{B} & 0 & & 0 & 0 \\ \mathbf{B} & \mathbf{C_2} & \mathbf{B} & 0 & & 0 \\ 0 & \mathbf{B} & \mathbf{C_3} & \mathbf{B} & 0 & \\ & 0 & & & & 0 \\ 0 & & 0 & \mathbf{B} & \mathbf{C_{P-1}} & \mathbf{B} \\ 0 & 0 & & 0 & \mathbf{B} & \mathbf{C_P} \end{bmatrix} \begin{bmatrix} \Psi_1^l \\ \Psi_2^l \\ \Psi_3^l \\ \vdots \\ \Psi_{P-1}^l \\ \Psi_P^l \end{bmatrix}, \tag{2.11}$$

which can be written symbolically as

$$\mathbf{A}\Psi^{l+1} = \mathbf{C}\Psi^l \text{ with } \Psi^l = \begin{bmatrix} \Psi_1^l \\ \vdots \\ \Psi_P^l \end{bmatrix}. \tag{2.12}$$

The right-hand side is known since $\mathbf{C}$ and Ψ^l (field values at the previous propagation step) are known. Solving this set of linear equations, the unknown field values in the next step are found. But, due to the artificial computational window radiated fields can always be present. To eliminate this, Absorbing Boundary Conditions (ABC's) or Transparent Boundary Conditions (TBC's) [20] are used with these linear equations. In addition, efficient interface conditions are applied [21]. These boundary and interface conditions are described in later sections.

If there is only one transverse dimension , i.e, the problem is two-dimensional, (2.2) reduces to the following equation :

$$2jk_o n_o \frac{\partial \psi}{\partial z} = \frac{\partial^2 \psi}{\partial x^2} + k_o^2[n^2(x,z) - n_o^2]\psi. \tag{2.13}$$

Then, $\Psi_p^l \rightarrow \psi_p^l$,$\mathbf{A_p} \rightarrow a_p$,$\mathbf{C_p} \rightarrow c_p$, $\mathbf{B} \rightarrow 1/2\Delta X^2$ and (2.10) reduces to a simple difference equation along x :

$$-\frac{1}{2\Delta X^2}\psi_{p-1}^{l+1} + a_p\psi_p^{l+1} - \frac{1}{2\Delta X^2}\psi_{p+1}^{l+1} = \frac{1}{2\Delta X^2}\psi_{p-1}^{l} + c_p\psi_p^{l} + \frac{1}{2\Delta X^2}\psi_{p+1}^{l}. \tag{2.14}$$

So, **A** becomes a tridiagonal matrix which can be solved using very efficient algorithms [19]. Therefore, it is very advantegous to convert a three-dimensional problem into a two-dimensional problem using the effective index approximation (see Sec.2.7), if possible. In full three dimensional case, it is better to use iterative techniques rather than the inversion of matrix **A** at each step.

In the case of TM modes, i.e., $H_y = \psi exp(-jk_o n_o z)$ the right-hand side of the paraxial wave equation should include the following expression (in two-dimensional case)

$$-\frac{\partial ln(n^2)}{\partial x}\frac{\partial \psi}{\partial x}. \tag{2.15}$$

Introducing a uniform discretization with step sizes Δx and Δz, and integrating in the interval $[l\Delta z, (l+1)\Delta z]$, using Crank-Nicholson scheme, it follows that

$$-b_p\psi_{p-1}^{l+1} + a_p\psi_p^{l+1} - \psi_{p+1}^{l+1} = b_p\psi_{p-1}^{l} + c_p\psi_p^{l} + \psi_{p+1}^{l}, \tag{2.16}$$

where

$$\begin{aligned}
a_p &= 2 + d_p - k_o^2\left(\frac{(n_{p,q}^{l+1})^2 + (n_{p,q}^{l})^2}{2} - n_o^2\right)\Delta x^2 + 4jk_o n_o \Delta x^2/\Delta z, \\
c_p &= -(2+d_p) + k_o^2\left(\frac{(n_{p,q}^{l+1})^2 + (n_{p,q}^{l})^2}{2} - n_o^2\right)\Delta x^2 + 4jk_o n_o \Delta x^2/\Delta z, \\
b_p &= 1 + d_p, \\
d_p &\simeq \frac{n_{p+1}^2 - n_p^2}{n_p^2}.
\end{aligned}$$

2.3 Explicit Finite Difference Beam Propagation Method

In explicit finite difference method (EFD-BPM), the paraxial wave equation is approximated like in the case of implicit FD-BPM, but to approximate $\frac{\partial \psi}{\partial z}$, second order accurate center difference approximation is used [12]. Then paraxial wave equation can be written as

$$\frac{\psi(z+\Delta z)-\psi(z-\Delta z)}{2\Delta z} = \frac{F\psi(z)}{jk_o n_o}, \tag{2.17}$$

where

$$F = \frac{\partial^2}{\partial x^2} + \frac{\partial^2}{\partial y^2} + k_o^2(n^2(x,y,z) - n_o^2). \tag{2.18}$$

Replacing the derivatives in F by finite difference approximations, the paraxial wave equation can be approximated as

$$\psi_{pq}(z+\Delta z) = \psi_{pq}(z-\Delta z)+a[\psi_{(p-1)q}(z)+\psi_{(p+1)q}(z)]+b[\psi_{p(q-1)}(z)+\psi_{p(q+1)}(z)]+c_{pq}\psi_{pq}(z). \tag{2.19}$$

where

$$\begin{aligned} a &= \frac{\Delta z}{jk_o n_o \Delta x^2}, \\ b &= \frac{\Delta z}{jk_o n_o \Delta y^2}, \\ c_{pq} &= \frac{\Delta z}{jk_o n_o}\left[-\frac{2}{\Delta x^2} - \frac{2}{\Delta y^2} - k_o^2(n_{pq}^2(z) - n_o^2)\right]. \end{aligned}$$

In (2.19), $\psi_{pq}(z)$ and $n_{pq}(z)$ are the field values and the sampled refractive index values, respectively, at $x = p\Delta x$ and $y = q\Delta y$ in the computational window. One can find the optical field distribution after Δz propagation by a direct matrix

multiplication of the ψ with a sparse matrix which has only five non-zero elements in each row.

The following condition assures both the stability and the power conservation in EFD-BPM [12] :

$$\Delta z < 2k_o n_o \left\{ \frac{4}{\Delta x^2} + \frac{4}{\Delta y^2} + k_o^2 |n_{pq}^2 - n_o^2| \right\}^{-1} \tag{2.20}$$

2.4 Applicability of FD-BPM

The effect of slowly varying amplitude approximation and the discretization along the z axis will be discussed for TE polarization for two-dimensional case (the TM case being similar).

To approximate the structure sufficiently accurate, it is assumed that the stepsize along the propagation direction, Δz, is small enough. For each step in the propagation direction, the structure can be considered to be z-independent and the field pattern can be decomposed into modal fields. Consider a modal field, $\xi(x)$, corresponding to [21]

$$\frac{\partial^2 \xi}{\partial x^2} + k_o^2 (n^2 - n_e^2)\xi = 0, \tag{2.21}$$

where n_e is the effective index, propagates according to the FD-BPM algorithm. Suppose that this modal field is propagated correctly except with respect to the phase, i.e.,

$$E(x,z) = \xi(x) exp\,[-jk_o(n_e + \Delta n)z] = \psi(x,z) exp(-jk_o n_o z). \tag{2.22}$$

Using (2.13), (2.21), (2.22), it follows that

$$\Delta n = (n_e - n_o)^2/2n_o. \tag{2.23}$$

Substituting (2.22) and (2.23) into (2.13), it follows that ψ which is defined by (2.22) is a solution of (2.13).

Equation (2.23) gives the error which results from the difference between the mode index and the reference refractive index. The nonvanishing stepsize, Δz, also introduces some error. Substituting (2.21)-(2.23) into (2.13), we obtain

$$\frac{\partial \psi}{\partial z} = -jk_o \left[(n_e - n_o) + \frac{(n_e - n_o)^2}{2n_o}\right]\psi = -jk_o \frac{(n_e^2 - n_o^2)}{2n_o}\psi \equiv -j\alpha\psi. \tag{2.24}$$

Integrating as in Sec.2.2 gives

$$\psi^{l+1} - \psi^l = -j\alpha \frac{(\psi^{l+1} + \psi^l)\Delta z}{2}. \tag{2.25}$$

So,

$$\psi^{l+1} = \left[\frac{2 - j\alpha\Delta z}{2 + j\alpha\Delta z}\right]\psi^l \equiv \psi^l exp(-j\gamma\Delta z), \tag{2.26}$$

whereas the solution according to (2.24) would be

$$\psi^{l+1} = \psi^l exp(-j\alpha\Delta z). \tag{2.27}$$

Note that Crank-Nicholson scheme leads to a solution of (2.24) correct up to second order in $\alpha\Delta z$ and in the absence of any absorption, the norm of the field is preserved. For the detailed power conservation analysis, the reader is referred to the literature [12].

From (2.22) the correct propagation ($\Delta n = 0$) of the field would be described by

$$\psi^{l+1} = \psi^l exp\left[-jk_o(n_e - n_o)\Delta z\right]. \tag{2.28}$$

Comparing (2.28) and (2.26), it follows that the following requirement should be fulfilled

$$n_o \simeq n_{e,m}, \tag{2.29}$$

where $n_{e,m}(m = 1, 2, ...)$ are the effective indexes of the mode involved and m shows the mode index. (2.29) is a fundamental requirement and limits the general applicability of the algorithm. In order to reduce possible errors due to deviations of (2.29), the following should hold

$$|\alpha \Delta z| \ll 1, \tag{2.30}$$

or,

$$k_o \Delta z \ll \frac{1}{|n_e - n_o|}. \tag{2.31}$$

If a single mode is launched into a z-invariant structure and $n_o = n_e$, the stepsize, Δz, can be chosen arbitrarily large. In addition, from (2.29), it may be deduced that the propagation should be rather close to paraxial [21].

2.5 Absorbing Boundary Conditions

BPM uses computational window which should be large enough to contain the desired field distribution all along the propagation path. Since radiated fields can always be present, setting the field values to zero at the boundaries of the computational window can create unphysical oscillations. This boundary condition creates reflecting boundary and causes the radiated fields to be reflected back and therefore yields spurious field distribution.

One way to prevent these oscillations is to use absorbing boundaries. In this method, an artificial complex index distribution around the computational

window is introduced to generate a lossy boundary. By this way, the radiated fields are absorbed before reaching the edge of the window. In practice, less than 10 mesh points around the boundary with a complex index is sufficient. To avoid reflections, the imaginary part of the index is tapered. Note that, the absorber should be kept outside of the desired field profile.

2.6 Efficient Interface Conditions

In BPM, using a discretization of the computational window, the true interface cannot always coincide with a mesh point. This fact may introduce errors. By adapting the refractive index at the mesh points in the vicinity of interfaces, the accuracy can be improved [21].

Consider an interface coinciding with a mesh point, say at $x_j = j\Delta x$. The fields near the interface should behave like $exp(\pm\gamma_p(x - x_j))$, in which the subscript $p = r, l$ for the right and left side of the interface, respectively, with $\gamma_p^2 = k_o^2(n_o^2 - n_p^2)$. Using the correct interface conditions, i.e, $\psi_l = \psi_r$ (TE,TM), $(\partial\psi/\partial x)_l = (\partial\psi/\partial x)_r$ (TE) and $n_r^2(\partial\psi/\partial x)_l = n_l^2(\partial\psi/\partial x)_r$ (TM), and discretization of the modal field equation

$$\frac{\partial^2\psi}{\partial x^2} + k_o^2(n^2 - n_o^2)\psi = 0, \tag{2.32}$$

we obtain the refractive index at the interface as follows :

$$n_{j,a}^2 = (n_r^2 + n_l^2)/2 + d_j(n_l^2 - n_o^2)/2 \tag{2.33}$$

with

$$\begin{aligned} d_j &= 0 \text{ (TE)}, \\ d_j &= (n_r^2 - n_l^2)/n_l^2 \text{ (TM)}. \end{aligned}$$

The interface lying between two mesh points can be treated similarly. Consider an interface between x_j and x_{j+1} at a distance $\zeta\Delta x$ from x_j. It can be found

$$n_{j,a}^2 = (n_j^2+n_{j+1}^2)/2+d_j(n_j^2-n_o^2)/2+\zeta(n_j^2-n_{j+1}^2)+\zeta d_j(n_j^2-n_o^2)+\zeta^2(n_{j+1}^2-n_j^2)/2 \tag{2.34}$$

with

$$\begin{aligned} d_j &= 0 \text{ (TE)}, \\ d_j &= (1-\zeta)(n_{j+1}^2 - n_j^2)/n_j^2 \text{ (TM)} , \end{aligned}$$

and

$$n_{j+1,a}^2 = n_{j+1}^2+d_{j+1}(n_o^2-n_{j+1}^2)/2+\zeta d_{j+1}(n_{j+1}^2-n_o^2)+d_{j+1}\zeta^2(n_j^2-n_{j+1}^2)/2+\zeta^2(n_j^2-n_{j+1}^2)/2 \tag{2.35}$$

with

$$\begin{aligned} d_j &= 0 \text{ (TE)}, \\ d_j &= \zeta(n_{j+1}^2 - n_j^2)/(n_{j+1}^2 + \zeta n_j^2 - \zeta n_{j+1}^2) \text{ (TM)}. \end{aligned}$$

Note that these formulas cannot be used in the presence of a second interface in the interval (x_{j-1}, x_{j+1}) without detailed information on the modes involved. In other words, in order to use these formulas the step size Δx should be chosen small enough so that more than one mesh point lies in a given layer.

2.7 The Effective Index Method

The effective index method has been used since the beginnings of integrated optics. The method is helpful in the understanding of structures. It has been proposed for the approximate analysis of channel guides by Knox and Toulios [1], and has produced results which were in good agreement with more exact computer results and experimental results for some practical structures such as ridge guides , buried channel guides and diffused channel guides.

The effective index approach starts with a birds-eye view of a planar film guide, with the film in the y-z plane. The guide is viewed in the x-direction. A uniform planar guide can be seen with a uniform effective index N independent of y and z. Small variations either in the guide thickness or in the refractive indices result an effective index pattern $N(y,z)$. When this pattern has the same shape of a familiar bulk optical component, analogy arguments are used to understand its characteristics. For a channel guide, the viewer sees the pattern reminiscent of a planar film guide with the film in the x-z plane. This is used to predict the modal fields and the propagation constants of the channel guide.

The effective index method for a general channel guide shown in Figure 2.1 proceeds with the following steps [22]:

1. Determine the normalized thickness V_f and V_l of the channel and lateral guides

$$V_f = kh\sqrt{(n_f^2 - n_s^2)}, \tag{2.36}$$

$$V_l = kh\sqrt{(n_l^2 - n_f^2)}. \tag{2.37}$$

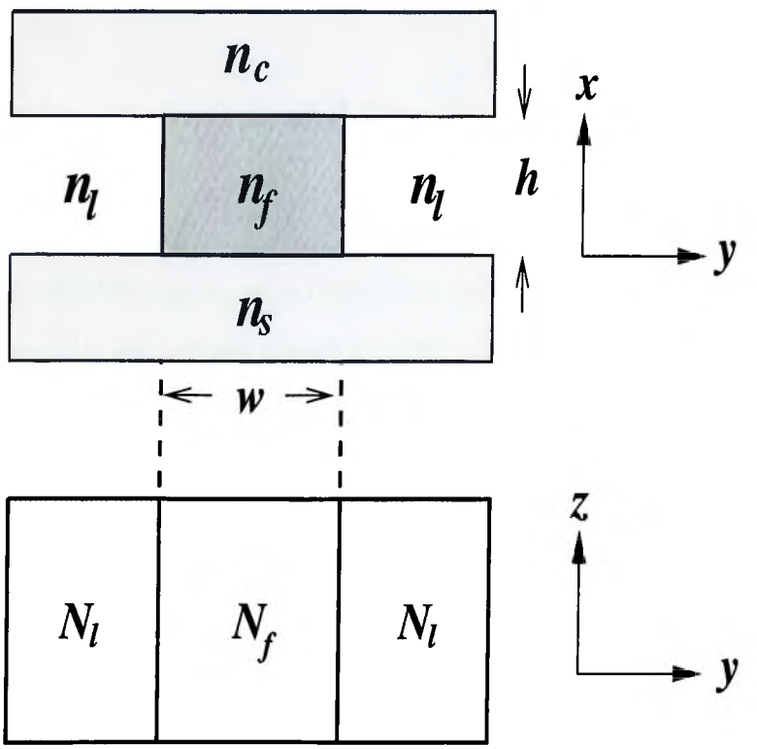

Figure 2.1: Illustration of the effective index method showing the cross section and the top view of a general channel guide

2. Use V-b diagrams to determine the normalized guide indices b_f and b_l of the two guides. To obtain V-b diagram for TE modes, use

$$V\sqrt{1-b} = \nu\pi + tan^{-1}\sqrt{b/(1-b)} + tan^{-1}\sqrt{(b+a)/(1-b)} \qquad (2.38)$$

where

$$V = kh\sqrt{n_f^2 - n_s^2}, \qquad (2.39)$$

$$b = \frac{N^2 - n_s^2}{n_f^2 - n_s^2}, \qquad (2.40)$$

$$a = \frac{n_s^2 - n_c^2}{n_f^2 - n_s^2}, \qquad (2.41)$$

and ν is the mode order. Determine the corresponding effective indices N_f

and N_l from

$$N_f^2 = n_s^2 + b_f(n_f^2 - n_s^2), \tag{2.42}$$

$$N_l^2 = n_s^2 + b_l(n_l^2 - n_s^2). \tag{2.43}$$

3. The method tells us to regard the slab guide suggested by the top view as equivalent to the actual channel guide. Determine the normalized width V_{eq} of the equivalent slab guide

$$V_{eq} = kw\sqrt{N_f^2 - N_l^2} = kw\sqrt{b_f(n_f^2 - n_s^2) - b_l(n_l^2 - n_s^2)}. \tag{2.44}$$

Now use V-b diagrams to determine the normalized guide index b_{eq} of the equivalent guide.

4. Determine the effective index N_{eq} of the equivalent guide and postulate its equality to effective index N of the channel guide :

$$N = N_{eq} = \sqrt{N_l^2 + b_{eq}(N_f^2 - N_l^2)}. \tag{2.45}$$

This provides a result for the effective index N and the propagation constant $\beta = kN$ of the channel guide.

Chapter 3

Orthogonal Bends

For practical realization of compact photonic integrated circuits, one often needs to change the direction of optical propagation in a short distance. To achieve this goal, smooth curved bends can be used. But it has been shown both experimentally and theoretically that small radii of curvatures can be realized using strongly guiding waveguides. In other words, smooth curved bends take up too much space, requiring as much as 1cm radius in weakly guiding waveguides in $Ti : LiNbO_3$ in order to have acceptable radiation loss [15]. Obviously this limits the packing density considerably. The most appropriate method for steering the optical propagation in a weakly guiding waveguide is to use an integrated optical corner reflector. It takes the advantage of total internal reflection at an etched interface between semiconductor and air.

Due to the large index difference between core and air at the corner, the reflection coefficient is very close to unity [23]. Such a bend can be characterized by an efficiency factor η_b, which accounts power loss as a result of the bend.

3.1 Analysis of Orthogonal Bend Using FD-BPM

The structure under consideration is a 90° semiconductor channel waveguide corner reflector. The cross-sectional profile of the general step index channel waveguides is shown in the inset of Figure 3.1. The channel guides are reduced to slab waveguides using effective index approximation. The geometry of Figure 3.1 represents the corner reflector [24]. The semiconductor-air interface obtained by etching acts like a mirror due to large index difference.

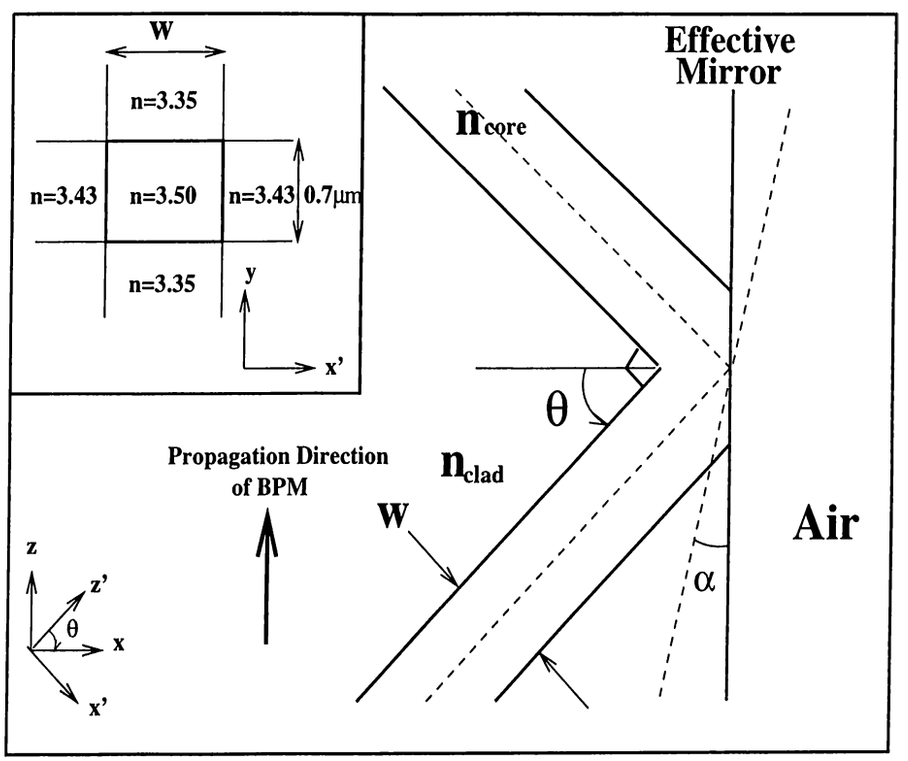

Figure 3.1: Integrated optical corner reflector studied in this work. The inset shows the cross-sectional profile of channel waveguide. The slab waveguide in the corner reflector is obtained from the channel waveguide using the effective index approximation.

In the analysis, it is assumed that the optical beam is propagating in the z-direction, which is parallel to the mirror interface. For accurate beam propagation in a tilted waveguide geometry, a proper value for the reference refractive index, n_o, should be chosen. It was pointed out in the literature that the most appropriate value for n_o in the paraxial approximation is $\beta sin\theta/k_o$ [25] where β is the propagation constant of the eigenmode of the slab waveguide and θ is the angle of incidence. An orthogonal bend which has two uniform waveguides tilted 45° is analyzed using implicit FD-BPM. At the input plane, i.e. $z = 0$, the following optical field distribution is launched:

$$E_y(x,z) = \Psi((x - x_o - zcot\theta)).exp(-j\beta(x - x_o - zcot\theta)cos\theta) \qquad (3.1)$$

where $\Psi(x - x_o)$ is the eigenmode of the slab waveguide which is represented by the index profile $n(x, z = 0)$. It is noted that the above expression is the transformation of z'-propagating eigenmode.

The corner reflector in Figure 3.1 is analyzed only for TE mode of the channel waveguide shown in the inset of Figure 3.1. Figure 3.2 shows the Gaussian wave propagation on the corner reflector structure. Note that, the semiconductor-air interface is placed at $x = 15\mu m$.

In the calculations, the wavelength is $1.5\mu m$, the computational window size and the number of mesh points in the x direction are $20\mu m$ and 2000 respectively. The propagation step size in the z-direction and the total propagation length in the positive z-direction are $0.1\mu m$ and $20\mu m$ respectively.

To find the efficiency factor, η_b, which accounts for the power loss as a result of the bend, remaining power in the core at the end of propagation distance is calculated to compare with the analytic results. Using the initial power in the

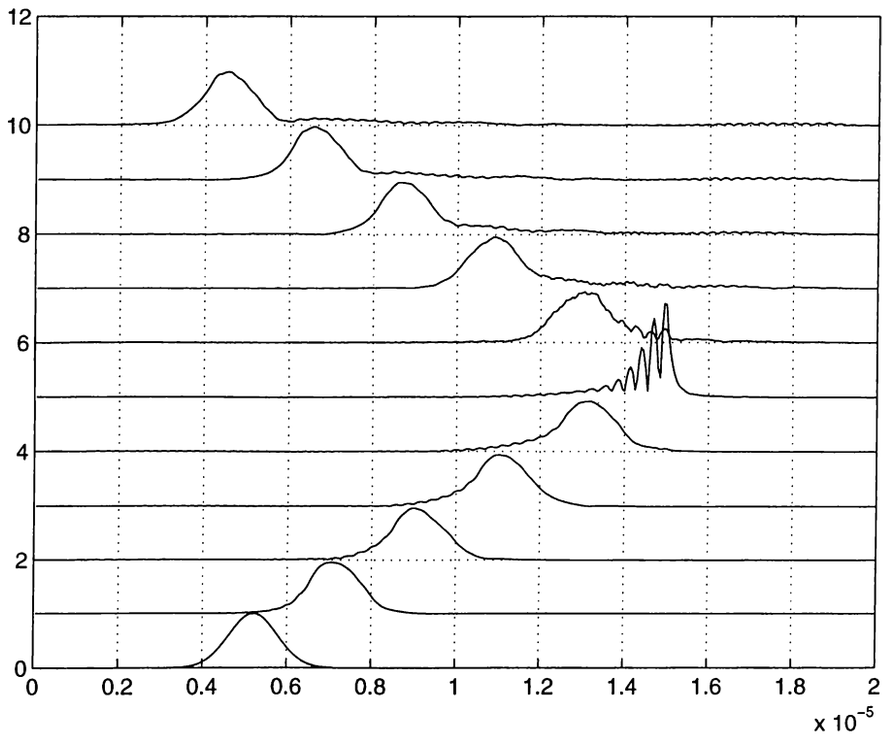

Figure 3.2: Gaussian beam propagation on the orthogonal bend structure.

core, η_b is calculated for different values of width. Figure 3.4 shows the efficiency factor for different waveguide widths. Note that for each different width values, the effective index method is applied again and the reference refractive index is found.

In addition, we study the effect of the rotation of the mirror from its ideal position by a tilt angle α as shown in Figure 3.1. The efficiency factors calculated using implicit FD-BPM for varying tilt angle, α, are plotted in Figure 3.5.

3.2 Analysis of Orthogonal Bend Using Fields of Shadows Method

The efficiency factor accounts for the power loss as a result of the bend. The loss can be mostly attributed to the power traveling outside the core, which can not be perfectly reflected. This suggests an approximate way of calculating the efficiency factor [26].

For the calculation of the percentage of power propagating in the core region, one can use Marcatili's "Fields of Shadows" method [27], in which, the waveguide is separated into two symmetric slab waveguides as shown in Figure 3.3. The refractive index of the shaded regions is $\sqrt{n_2^2 + n_3^2 - n_1^2}$. This method is very accurate for well-guided case. When the indices of the shaded regions are deviated from $\sqrt{n_2^2 + n_3^2 - n_1^2}$, the error made in this method starts to increase.

For a symmetric step index slab waveguide, the following eigenvalue equation for the weakly-guiding fundamental mode is solved numerically for β:

$$t\sqrt{k_o^2 n_{co}^2 - \beta^2} = 2tan^{-1}\sqrt{\frac{\beta^2 - k_o^2 n_{cl}^2}{k_o^2 n_{co}^2}} \Leftrightarrow W = UtanU \tag{3.2}$$

where

$$V = k_o \frac{t}{2}\sqrt{n_{co}^2 - n_{cl}^2}, \tag{3.3}$$

$$U = \frac{t}{2}\sqrt{k_o^2 n_{co}^2 - \beta^2}, \tag{3.4}$$

$$W = \frac{t}{2}\sqrt{\beta^2 - k_o^2 n_{cl}^2}, \tag{3.5}$$

t is the thickness of the core region, k_o is the wave number in the vacuum.

The percentage of power propagating in the core region for TE modes can be

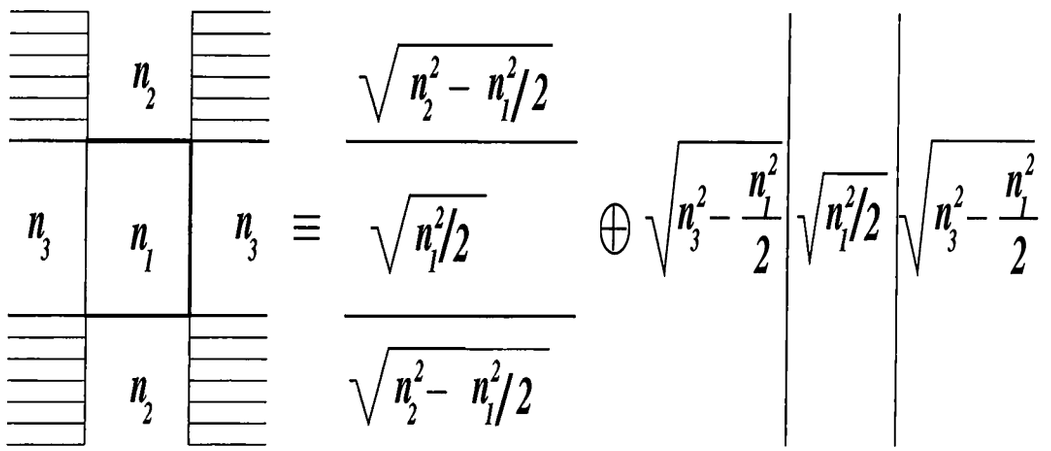

Figure 3.3: Separation of a channel waveguide into two symmetric step index slab waveguide.

calculated by [18]

$$\eta = 1 - \frac{U^2}{V^2(1+W)} \tag{3.6}$$

which is approximately equal to η_b for the weakly guiding waveguide.

Using this formula, the efficiency factor is calculated and plotted in Figure 3.4 for different width values.

3.3 Comparison

The efficiency factors calculated using FD-BPM for different values of width are found to be in good agreement with the asymptotic results on the same structure. For widths smaller than 0.7 μm the difference between both results are large. The reason of this difference is that for those width values a single mode waveguide does not exist physically.

Both results show that as the width of guide increases the efficiency factor increases. For this geometry, FD-BPM can be used for widths between 0.7 μm and 1.1 μm accurately and efficiently as it can be seen from Figure 3.4.

The advantage of FD-BPM can be easily seen in Figure 3.5. The rotation angle of the mirror surface affects the efficiency factor. But the asymptotic solution does not take into account this effect. In other words, for different rotation angles of mirror surface, efficiency factor is the same. But FD-BPM results show that as the rotation angle of mirror surface increases the efficiency factor decreases. However for angles smaller than 0.1°, the loss is smaller than 0.2 dB. and since the alignment of rotation with an accuracy of 0.1° can be easily achieved [24], in the design of corner reflector, less attention must be paid to reducing rotation error.

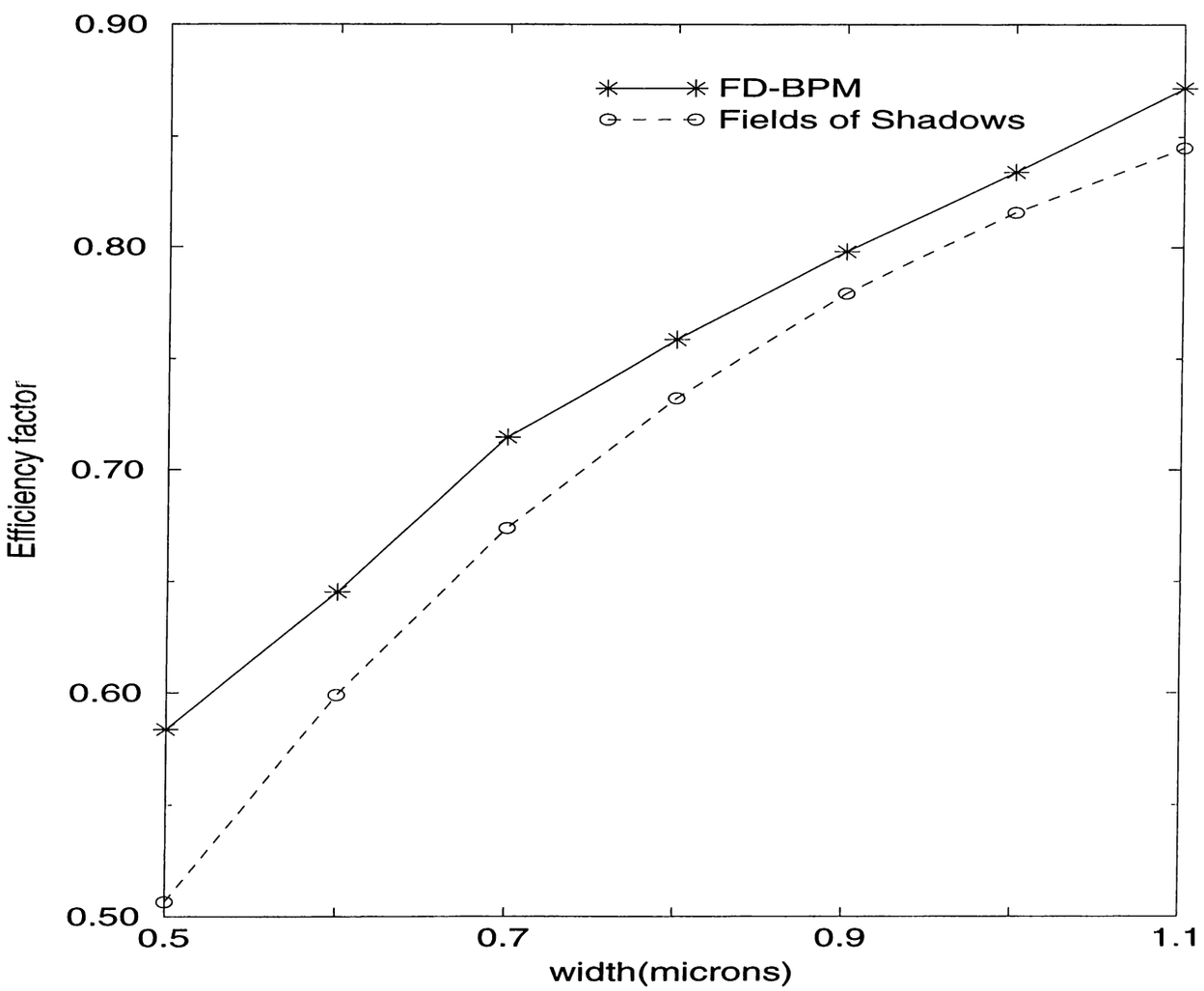

Figure 3.4: Efficiency factor for different values of width.

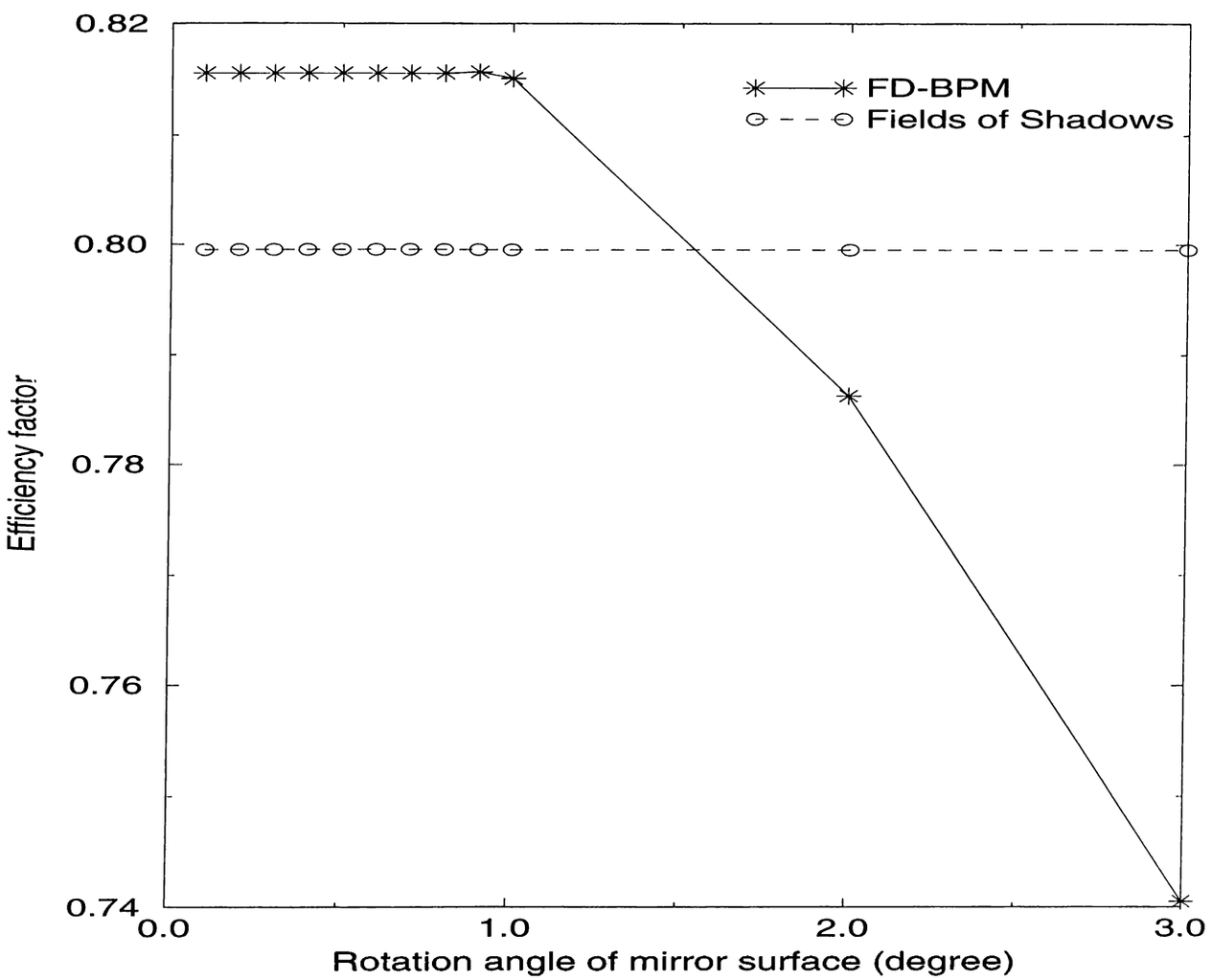

Figure 3.5: Efficiency factor for different tilt angles.

Chapter 4

Curved Coupler Structure

Transfer of power between two or more waveguides is an essential function required in integrated circuits that employ planar dielectrics as guiding media. A directional coupler is such a device that distributes the power from the input guide to one or more output guides in a controlled manner. Due to this important role, a typical integrated circuit consists of several couplers. In addition, in such integrated circuits, some interconnections act like couplers unintentionally. For these reasons, it is necessary to study the coupling characteristics of these couplers in great detail.

Various analyses for the coupling characteristics of the dielectric waveguides have been done by several authors (see Mittra [17] and the references therein) and in many of these studies scattering coefficients are found and it is an easy exercise to calculate power transfer ratios from the scattering coefficients. In this chapter, one of the nonparallel coupling structures, a curved coupler structure, is analyzed using both the coupled-mode theory of electromagnetics and the implicit

FD-BPM. In practice, the symmetric coupler with nonuniform coupling spacing is one of the popular configurations.

4.1 Analytic Solution of Curved Coupler Structure

4.1.1 Parallel Directional Couplers

A simple parallel directional coupler with length l is shown Figure 4.1. Due to the symmetry about $x = 0$ plane, the propagating modes of this structure are either symmetric (k_{even}) or antisymmetric (k_{odd}). These two wave numbers are approximately given as [17]:

$$k_{even} = k_z \left[1 + 2\frac{k_x^2 \xi exp(-d/\xi)}{k_z^2 a(1 + k_x^2 \xi^2)}\right], \tag{4.1}$$

$$k_{odd} = k_z \left[1 - 2\frac{k_x^2 \xi exp(-d/\xi)}{k_z^2 a(1 + k_x^2 \xi^2)}\right], \tag{4.2}$$

where k_x and k_z are the transverse and longitudinal propagation constants of a single guide respectively and derived using the generalized effective dielectric constant method; d is the spacing between the two guides; a is the guide width; and ξ is the field decay coefficient

$$\xi = \left[(\epsilon_{re}(y) - 1)k_o^2 - k_x^2\right]^{-1/2}. \tag{4.3}$$

The relative dielectric constant of the material is replaced by the effective dielectric constant which is given as

$$\epsilon_{re}(y) = \epsilon_r - (k_y/k_o)^2. \tag{4.4}$$

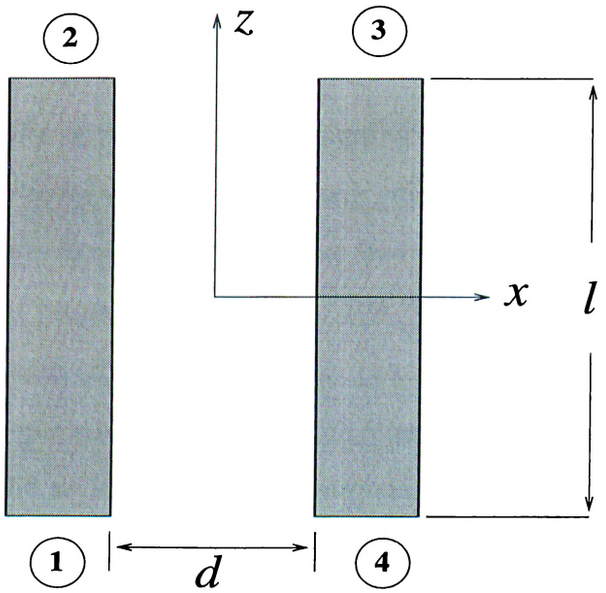

Figure 4.1: Parallel coupling structure.

k_y is obtained by the generalized effective dielectric constant method. A brief description of the effective dielectric constant method is given in the next section.

Finally, the scattering coefficients for the coupling section can be expressed as [17]

$$|S_{21}| = \left| cos \frac{k_{even} - k_{odd}}{2} l \right|, \tag{4.5}$$

$$|S_{31}| = \left| sin \frac{k_{even} - k_{odd}}{2} l \right|, \tag{4.6}$$

where l is the total coupling length of the coupling section, and $(k_{even} - k_{odd})/2$ is defined as the coupling coefficient. By taking the square of these equations, the power transfer ratios are easily obtained.

4.1.2 Nonparallel Symmetric Couplers

A symmetric coupler with nonuniform coupling spacing is shown in Figure 4.2. Each arm is made up of a circular dielectric guide of mean radius R and width a. In a dielectric waveguide, the equiphase fronts of the propagating modes are normal to the axial propagation direction. But, with the existence of the second waveguide, it is assumed that these fronts can be approximated by cylindrical planes [17]. The separation between the incremental coupling length of the two lines is given by the arclength L. The summation of coupling from these incremental coupling lengths gives the total coupling of two lines. The spacing d in (4.1) and (4.2) is replaced by L which is given by

$$L = 2r\theta, \tag{4.7}$$

where θ is the angle from the incremental coupling length to the center line, and

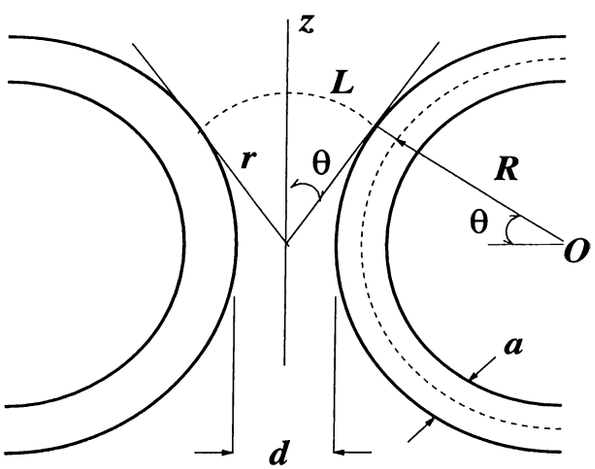

Figure 4.2: Nonparallel symmetric coupler.

r is the radius of cylindrical phase front which can be expressed as follows :

$$r = \frac{d_o/2 + (R + a/2)(1 - cos\theta)}{sin\theta}, \tag{4.8}$$

where d_o is the smallest spacing between two curved guides.

By substituting (4.7), (4.8), (4.1) and (4.2) into (4.5) and (4.6) and using $dl = Rd\theta$, we get [17]

$$|S_{21}| = |cos(KI_s)|, \tag{4.9}$$

$$|S_{31}| = |sin(KI_s)|, \tag{4.10}$$

where

$$K = \frac{4k_x^2 \xi R}{k_z a(1 + k_x^2 \xi^2)}, \tag{4.11}$$

$$I_s = \int_0^{\pi/2} exp\left[-\frac{\theta\{d_o + 2(R + a/2)(1 - cos\theta)\}}{\xi sin\theta}\right] d\theta. \tag{4.12}$$

4.1.3 Generalized Effective Dielectric Constant Method

In general, the effective dielectric constant $\epsilon_{re}(y)$ is defined as [17]

$$\epsilon_{re}(y) = (k_z/k_o)^2 = \epsilon_r - (k_y/k_o)^2, \tag{4.13}$$

where ϵ_r is the relative permittivity of the dielectric material; k_y is the transverse propagation constant of a dielectric slab of thickness b; and k_o is the free-space wave number.

The axial propagation constant of the original guide is given by

$$k_z^2 = \epsilon_{re}(y)k_o^2 - k_x^2, \tag{4.14}$$

where k_x is the transverse propagation constant of a dielectric slab of thickness a and permittivity $\epsilon_{re}(y)$; and k_x satisfies

$$\epsilon_{re}(y)k_o^2 - k_x^2 = k_o^2 + 1/\xi^2, \tag{4.15}$$

where

$$\xi = \left((\epsilon_{re}(y) - 1)k_o^2 - k_x^2\right)^{-1/2}. \tag{4.16}$$

ξ is the decay coefficient in the x-direction in the air medium.

By this way, k_x can be obtained from k_y through the effective dielectric constant $\epsilon_{re}(y)$.

Similarly, this sequence can be reversed. First k_x is solved for a dielectric slab of thickness a and relative permittivity ϵ_r. The new effective dielectric constant is

$$\epsilon_{re}(x) = \epsilon_r - (k_x/k_o)^2. \tag{4.17}$$

The axial propagation constant for this case is obtained by

$$k_z^2 = \epsilon_{re}(x)k_o^2 - k_y^2 = k_o^2 + 1/\eta^2, \tag{4.18}$$

where k_y is the transverse propagation constant of a dielectric slab of thickness b and relative dielectric constant $\epsilon_{re}(x)$; and

$$\eta = \left((\epsilon_{re}(x) - 1)k_o^2 - k_y^2\right)^{-1/2}. \tag{4.19}$$

η is the field decay coefficient in the y-direction in the air medium.

These two approaches are combined to obtain a "generalized" effective dielectric constant method. The dielectric waveguide is first converted into an infinite

slab in x to obtain k_{y1}. k_{x1} is then obtained from k_{y1} using $\epsilon_{re}(y)$. A new value k_{y2} is obtained from k_{x1} using $\epsilon_{re}(x)$. Then k_{x2} is obtained from k_{y2} using $\epsilon_{re}(y)$ again, and so on. After a few iterations, the transverse propagation constants k_{xn} and k_{yn} will converge, and using these values, the final longitudinal propagation constant k_z is derived.

4.1.4 Results

First, using generalized effective dielectric method, wave numbers are calculated. The guide dimensions are 2.27x1.0cm, $R = 21.42cm$ and $\epsilon_r = 2.6$. Using the integration equation (4.12), the summation of the couplings of all incremental coupling lengths is calculated for f = 8.5GHz. For different guide spacing d, P_{21} and P_{31} (remaining and transferred power respectively) are calculated and plotted as shown in Figure 4.6 and denoted also as Mittra on the figure. It is assumed that for the large radius R, the wave numbers of both guides can be roughly equal to that of straight guide.

4.2 Analysis of Curved Coupler Structure Using FD-BPM

The structure considered in this study is composed of two circularly curved single mode waveguides with curvature R as shown in Figure 4.3. The branches of the structure are separated by a minimum distance d and are symmetric with respect to the origin. The cross-sectional profile of the waveguides is rectangular. The

guide dimensions are 2.27x1.0cm; $R = 21.42cm$ and $\epsilon_r = 2.6$. Note that, these values are the same as the coupler structure studied in Sec.4.1.

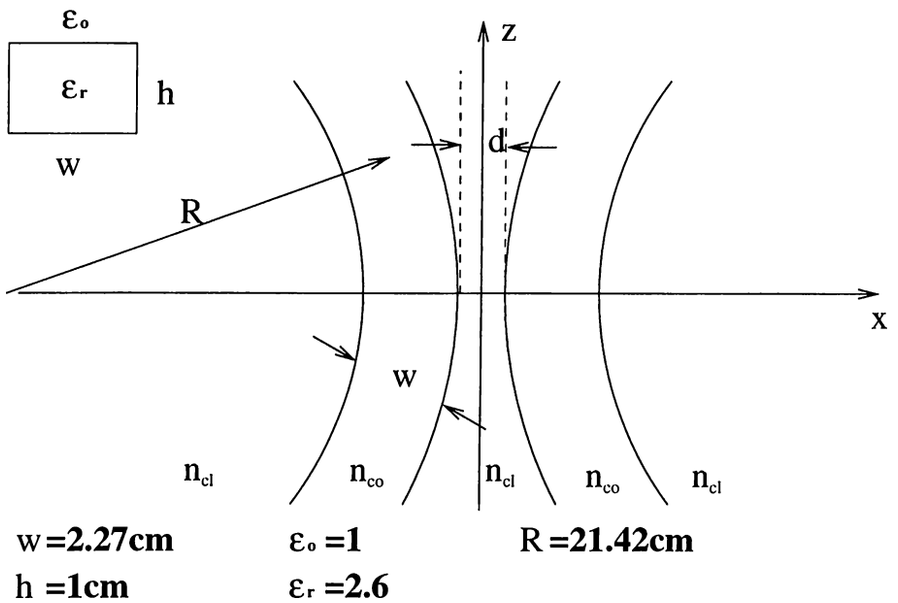

Figure 4.3: Curved coupler structure studied in this work.

Using effective index approximation, the rectangular guides are reduced to slab curved guides. In other words, the 3-D geometry is converted into a 2-D geometry.

In order to get accurate results, reference refractive index value, n_o, should be chosen carefully. The propagation of an eigenmode in one of the arm of the curved coupler structure is considered to specify the reference index value. At the input, the eigenmode propagating in the direction of waveguide is launched. For various values of reference index, the overlap integral of the optical field at the output of the waveguide with the input field profile is calculated using implicit FD-BPM. In the calculation, the window size is $L_x = 20cm$, and the number of mesh points is $M_x = 400$, and $\Delta z = 0.0325$. It is observed that the results

obtained from implicit FD-BPM are greatly dependent on the reference index but accurate for a proper reference index value.

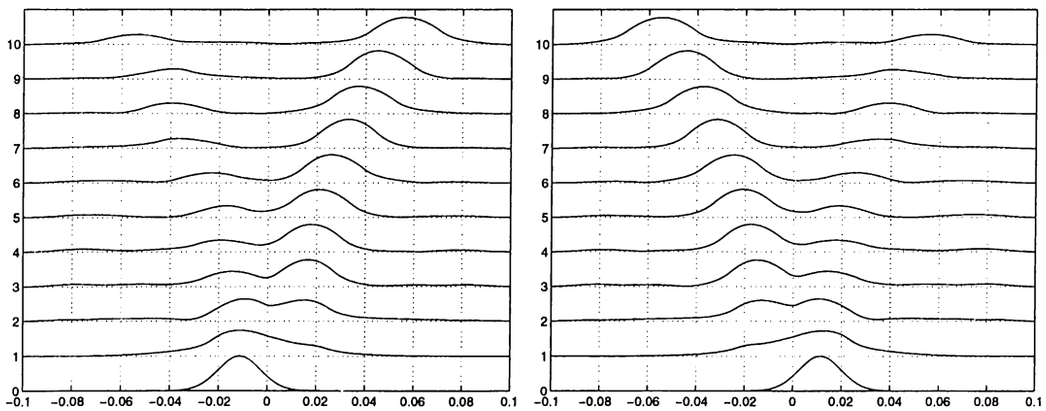

Figure 4.4: Gaussian beam propagation on the curved coupler structure

To confirm the accuracy, we have numerically validated the power conservation and symmetry considerations. A Gaussian beam is excited at each arm of the coupler separately and propagated through positive z-direction. Figure 4.4 shows the Gaussian beam propagation in the coupler structure for the excitement at the left and right arms respectively. As it can be seen from the plots, the propagation is symmetric with respect to the origin as expected.

Finally, power transfer ratios of the coupler are calculated using implicit FD-BPM. The eigenmode of the single mode waveguide is excited at the left arm of the coupler (at $z = -5cm$) and propagated in positive z-direction. Resulting output field is used to calculate remaining and transferred power at the output as shown in Figure 4.5.

For different minimum spacing values $P1$ and $P2$ defined in Figure 4.5 are calculated and plotted in Figure 4.6.

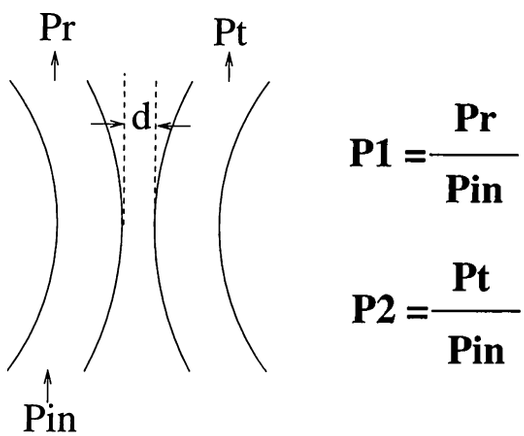

Figure 4.5: Power transfer ratio calculation

4.3 Comparison

Figure 4.4 shows the coupling of Gaussian wave excited on one of the arms of the structure into the other arm. As the distance between two curved section increases, the coupling decreases. After some distance, approximately $10cm$ in z-direction, no coupling observed, i.e., the peaks of the resulting field propagates independently. The symmetry property of the structure is observed from these figures. The plots are mirror images of each others. Also, the initial field is shifted from the center of the waveguides, a phenomena that has been pointed out several times in the literature [16].

The power transfer ratios calculated using implicit FD-BPM for different guide spacing, d, are in good agreement with the analytic solution developed by Mittra [17] and also discussed in Sec.4.1. Figure 4.6 shows the inverse relation between the guide spacing and $P2$, transferred power to the output guide. As the guide spacing increases most of the input power remain in the excited arm.

Finally, the sum of $P1$ and $P2$ values are nearly the same and equal to 1 for each values d. Both results are approximate but implicit FD-BPM gives an opportunity to see the evolution of the input field although Mittra's results give information about only the behavior of the field at the end of the propagation.

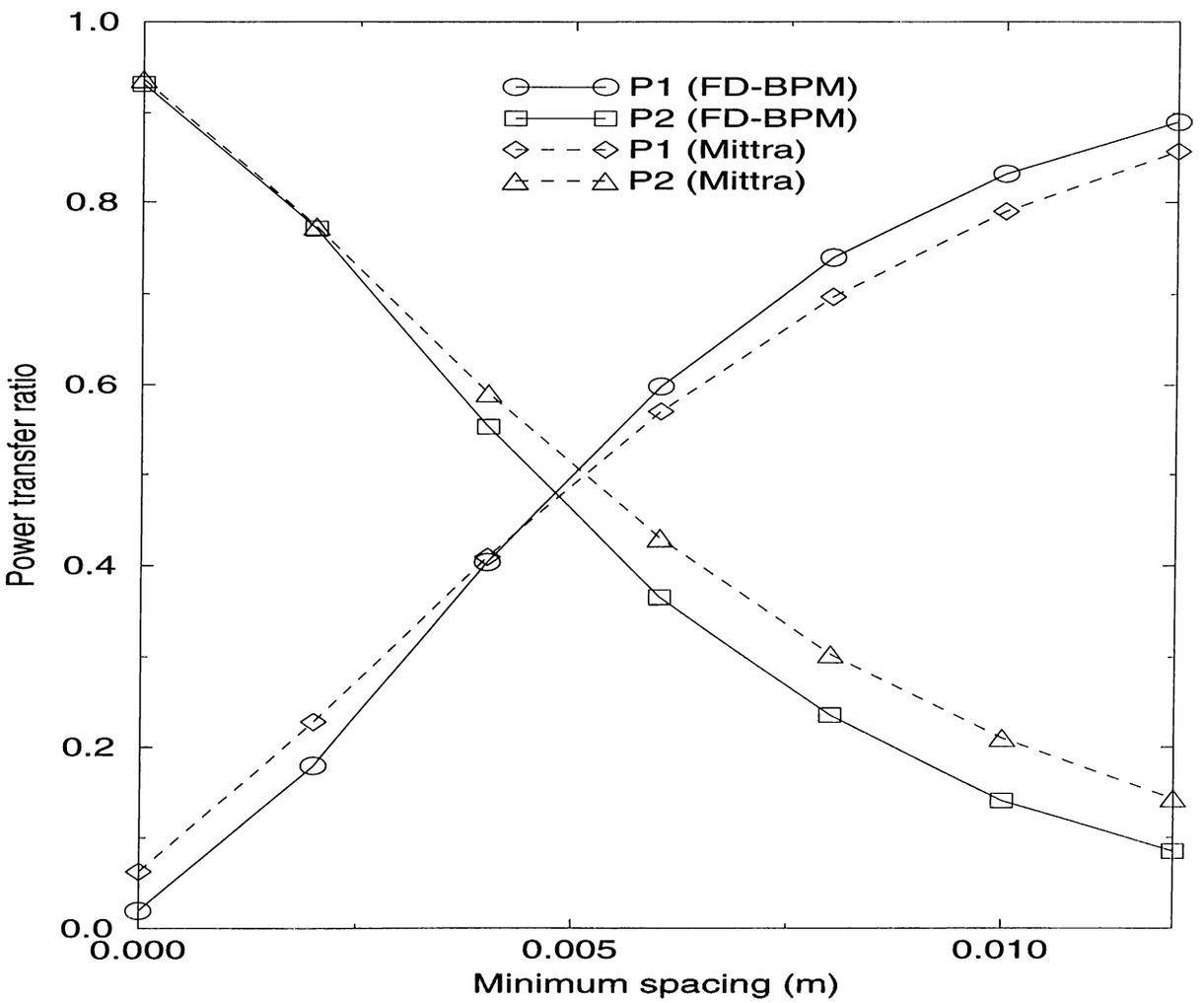

Figure 4.6: Power transfer ratios

Chapter 5

Conclusions

In this thesis, implicit FD-BPM is used for analysis of two z-variant dielectric structures. Although the method has some limitations , the implementation and the idea behind it are very simple. It is user friendly and very accurate. Both z-invariant and z-variant structures can be analyzed efficiently. In addition, the evolution of the input field is easily observed. With the help of some other basic methods such as effective index method, CPU performance can be increased. To sum, if the properties of the structure under consideration satisfy the requirements of the FD-BPM, the method is one of the best tools for analysis and design of integrated optical structures.

An orthogonal bend is one of the z-variant structures analyzed in the thesis. To change the direction of the wave in PIC, orthogonal bends are widely used. Investigation of bend loses and evolution of the field give some important information about the design and analysis of such structures. The efficiency factor

which accounts bend loss, characterizes orthogonal bends. For a single-mode orthogonal bend, it is observed that as the width of the waveguide increases the efficiency factor takes higher values, i.e., the bend loss decreases. So, in the design of an orthogonal bend, the width of the structure is determined for desired efficiency factor using the efficiency factor versus width values plot.

In the analysis, the beam is propagated in the direction parallel to the etched semiconductor-air interface. Using this approach, the errors that results in fabrication process such as the roughness of the interface and the rotation of the mirror from its ideal position, are easily studied. The efficiency factor is calculated for some rotation angles and it's observed that the efficiency factor is nearly same for the angles smaller than 1° and for bigger angles, significant drop is observed in the efficiency. We conclude that, in the fabrication process, the rotation angle should be smaller than 1° otherwise the efficiency factor deviates from the desired value.

Another z-variant structure analyzed in the thesis is a curved coupler structure. Besides its usage as a coupler, it can be considered as a model for some interconnections in integrated circuits. The branches of the structure are symmetric with nonuniform coupling length. In integrated circuits, some interconnections may have this configuration and as a result, the leakage of the field from one branch to the other branch occurs. So, the amount of the leakage and its dependence on the minimum distance between the branches are important design parameters of such circuits [26]. The power transfer ratios characterize the amount of remaining and transferred power in each branch. Using implicit FD-BPM, these ratios are calculated and for different minimum spacing values remaining and transferred power are found. The transferred power from input

waveguide to the output waveguide decreases, i.e., the remaining power increases as the minimum spacing of the structure increases. By this way, in the design of such structures, the minimum distance between the branches is determined for desired power transfer ratios.

In addition, the evolution of the input field through propagation in positive z-direction gives some information about the properties of resulting field. After some distance in z-direction, the coupling doesn't occur. Also, the field shifts from the center of the waveguide as it propagates. These two observation are advantages of the FD-BPM.

Finally, FD-BPM is one of the user friendly and effective tools in the design and analysis of components of integrated circuits. To examine the vectorial nature of the propagating field, vectorial FD-BPM will be used as a further improvement. Also, first-order and second-order correction of the method give much more accurate results [28].

Appendix A

Crank-Nicholson Scheme

Crank-Nicholson scheme is simply the average of the explicit and implicit Forward Time Center Space (FTCS) schemes as shown in Figure A.1. To illustrate its implementation, consider the following differential equation :

$$\frac{\partial u}{\partial t} = D\frac{\partial^2 u}{\partial x^2} \tag{A.1}$$

where D is a constant.

Using explicit FTCS scheme, it can be differenced as :

$$\frac{u_j^{n+1} - u_j^n}{\Delta t} = D\left[\frac{u_{j+1}^n - 2u_j^n + u_{j-1}^n}{(\Delta x)^2}\right]. \tag{A.2}$$

But according to von Neumann stability analysis, the stability criterion is :

$$\frac{2D\Delta t}{(\Delta x)^2} \leq 1 \tag{A.3}$$

which shows the maximum allowed timestep.

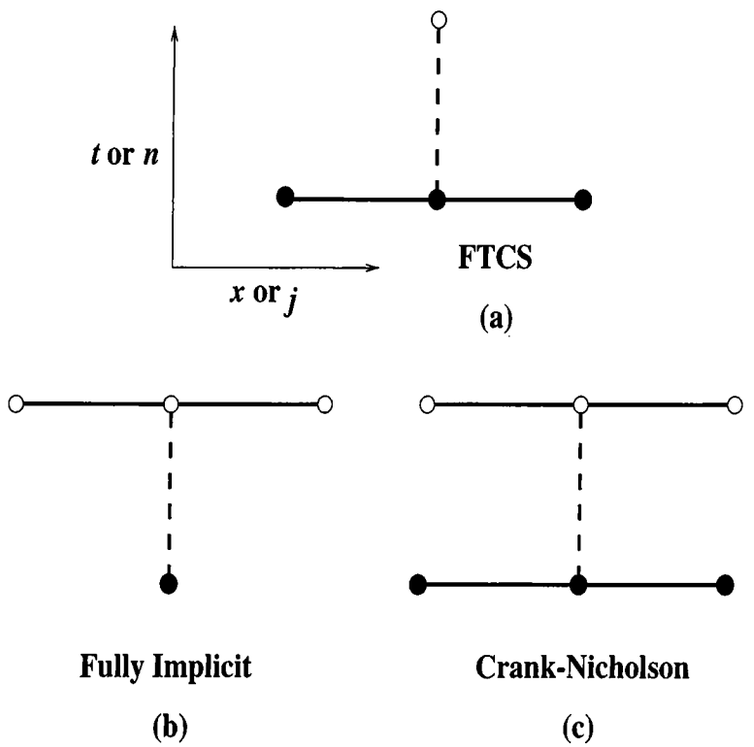

Figure A.1: Three differencing schemes. (a) Forward Time Center Space. (b) Fully Implicit. (c) Crank-Nicholson. The open circle is the new point at which the solution is desired; filled circles are used in calculating the new point; the solid lines connect points that are used to calculate the spatial derivatives; the dashed lines connect points that are used to calculate time derivatives.

Another differencing scheme is fully implicit or backward time scheme and according to this scheme, we get :

$$\frac{u_j^{n+1} - u_j^n}{\Delta t} = D\left[\frac{u_{j+1}^{n+1} - 2u_j^{n+1} + u_{j-1}^{n+1}}{(\Delta x)^2}\right]. \tag{A.4}$$

This is exactly like the FTCS scheme, except that the spatial derivatives on the right-hand side are evaluated at time step $n+1$. Again, using von Neumann stability analysis, it is concluded that for any stepsize, Δt, this scheme is unconditionally stable. But, with this scheme, the correct equilibrium solution is obtained which is the characteristic feature of implicit methods.

Finally, if we combine the stability of an implicit method with the accuracy of a method that is second-order in both space and time, we get Crank-Nicholson scheme. According to this scheme, (A.1) can be differenced as follows :

$$\frac{u_j^{n+1} - u_j^n}{\Delta t} = \frac{D}{2}\left[\frac{(u_{j+1}^{n+1} - 2u_j^{n+1} + u_{j-1}^{n+1}) + (u_{j+1}^n - 2u_j^n + u_{j-1}^n)}{(\Delta x)^2}\right]. \qquad \text{(A.5)}$$

Here, both the left- and right-hand sides are centered at timestep $n + \frac{1}{2}$, so the method is second-order accurate in time. The stability analysis shows that the scheme is unconditionally stable for any size Δz.

References

[1] R. M. Knox and P. P. Toulios "Integrated circuits for the millimeter through optical range," in *Proc., MRI Symposium on Submilimeter waves*, pp. 497–516, Brooklyn, NY: Polytechnical, 1970.

[2] M. J. Robertson, S. Ritche, and P. Dayan "Semiconductor waveguide: analysis of optical propagation in single rib structures and directional couplers," *Proc. IEE*, vol. 132, pp. 336–342, 1985.

[3] B. M. A. Rahman and J. B. Davies "Finite element analysis of optical and microwave waveguide problems," *IEEE Trans. Microwave Theory Tech.*, vol. MTT-32, pp. 20–28, Jan. 1984.

[4] M. D. Feit and J. A. Fleck Jr. "Computation of mode properties in optical fiber waveguides by the propagating beam method," *Appl. Opt.*, vol. 19, pp. 1154–1164, 1980.

[5] L. Thylen "The beam propagation method: an analysis of its applicability," *Opt. Quantum Electron.*, vol. 15, pp. 433–439, 1983.

[6] J. Van Roy, J. van der Donk, and P. E. Lagasse "Beam propagation method: analysis and assessment," *J. Opt. Soc. Am.*, vol. 71, pp. 803–810, 1983.

[7] D. Yevick and B. Hermansson "Split-step finite difference analysis of rib waveguides," *Electronics Letters*, vol. 25, pp. 461–462, 1989.

[8] D. Yevick and M. Glasner "Analysis of forward wide-angle light propagation in semiconductor rib waveguides and integrated-optics structures," *Electronics Letters*, vol. 25, pp. 1611–1612, 1989.

[9] D. Yevick and B. Hermansson "Efficient beam propagation techniques," *IEEE J. Quantum Electron.*, vol. 26, pp. 109–112, Jan. 1990.

[10] Y. Chung and N. Dagli "An assessment of finite difference beam propagation method," *IEEE J. Quantum Electron.*, vol. 26, pp. 1335–1339, 1990.

[11] Y. Chung and N. Dagli "An explicit finite difference beam propagation method: application to semiconductor rib waveguide Y-junction analysis," *Electronics Letters*, vol. 26, pp. 711–713, 1990.

[12] Y. Chung and N. Dagli "Analysis of z-invariant and z-variant semiconductor rib waveguides by explicit finite difference beam propagation method with nonuniform mesh configuration," *IEEE J. Quantum Electron.*, vol. 27, pp. 2296–2305, 1991.

[13] P. L. Liu, S. L. Yang, and D. M. Yuan "The semivectorial beam propagation method," *IEEE J. Quantum Electron.*, vol. 29, pp. 1205–1211, 1993.

[14] W. P. Huang, C. Xu, S. T. Chu, and S. K. Chaudhuri "The finite-difference vector beam propagation method: Analysis and assessment," *IEEE J. Lightwave Technol.*, vol. 10, pp. 295–305, 1992.

[15] G. Onal, A. Altintas, and H. M. Ozaktas "Computer-aided analysis and simulation of complex passive integrated optical circuits of arbitrary rectilinear topology," *Opt. Eng.*, vol. 33, pp. 1596–1603, 1994.

[16] M. Rivera "A finite difference BPM analysis of bent dielectric waveguides," *IEEE J. Lightwave Technol.*, vol. 13, pp. 233–238, 1995.

[17] T. Trinh and R. Mittra "Coupling characteristics of planar dielectric waveguides of rectangular cross section," *IEEE Trans. Microwave Theory Tech.*, vol. MTT-29, pp. 875–880, Sep. 1981.

[18] A. W. Snyder and J. D. Love. *Optical Waveguide Theory.* Chapman and Hall, New York, 1983.

[19] W. H. Press, B. P. Flannery, S. A. Teukolsky, and W. T. Vetterling. *Numerical Recipes: The Art of Scientific Computing.* Cambridge University Press, Cambridge, 1989.

[20] G. R. Hadley "Transparent boundary conditions to the beam propagation method," *IEEE J. Quantum Electron.*, vol. 28, pp. 363–370, 1992.

[21] H. J. W. M. Hoekstra, G. J. M. Krijnen, and P. V. Lambeck "Efficient interface conditions for the finite difference beam propagation method," *IEEE J. Lightwave Technol.*, vol. 10, pp. 1352–1355, 1992.

[22] Ed. T. Tamir. *Integrated Optics.* Springer-Verlag, New York, 1979.

[23] R. Sims and J. Cozens. *Optical Guided Waves and Devices.* McGraw-Hill, Shoppenhangers Road, Maidenhead, Bershire, England, 1992.

[24] Y. Chung and N. Dagli "Analysis of integrated optical corner reflector using finite-difference beam propagation method," *IEEE Photon. Technol. Lett.*, vol. 3, pp. 150–152, 1991.

[25] D. Yevick, C. Rolland, W. Bardyszewski, and B. Hermansson "Fresnel studies of reflected beams," *IEEE Photon. Technol. Lett.*, vol. 2, pp. 490–492, 1990.

[26] G. Onal. "Computer aided analysis and simulation of complex passive integrated optical circuits,". Master's thesis, Bilkent University, Ankara Turkey, June 1993.

[27] H. Kogelnik. *Guided-Wave Optoelectronics.* Springer-Verlag, Berlin, 1988.

[28] H. J. W. M. Hoekstra, G. J. M. Krijnen, and P. V. Lambeck "On the accuracy of the finite difference method for applications in beam propagating techniques," *Opt. Commun..*, vol. 94, pp. 506–508, 1992.